Available online at www.sciencedirect.com
SCIENCE DIRECT
Journal of Crystal Growth 291 (2006) 27–33
JOURNAL OF CRYSTAL GROWTH
www.elsevier.com/locate/jcrysgro

Temperature-dependent optical properties of $In_{0.34}Ga_{0.66}As_{1-x}N_x$/GaAs single quantum well with high nitrogen content for 1.55 μm application grown by molecular beam epitaxy

Fang-I. Lai[a,1], S.Y. Kuo[b], J.S. Wang[c,2], R.S. Hsiao[c], H.C. Kuo[a,*], J. Chi[c], S.C. Wang[a], H.S. Wang[d], C.T. Liang[d], Y.F. Chen[d]

[a]*Department of Photonics and Institute of Electro-optical Engineering, National Chiao-Tung University, 1001 Ta-Hsueh Rd, Hsinchu, 300 Taiwan*
[b]*Instrument Technology Research Center, National Applied Research Laboratories, Hsinchu, 300, Taiwan*
[c]*Opto-Electronics & System Laboratory, Industrial Technology Research Institute, Hsinchu County 310, Taiwan*
[d]*Department of Physics, National Taiwan University, Taipei, Taiwan*

Received 25 January 2005; accepted 20 February 2006
Communicated by C.R. Abernathy
Available online 18 April 2006

Abstract

The temperature dependence of optical properties of InGaAsN/GaAs single-quantum wells grown by solid source molecular beam epitaxy (MBE) with N contents varied from 0% to 5.3% was investigated by photoluminescence (PL). The evolution of the peak positions of InGaAs/GaAs sample are in agreement with the empirical Varshni model. However, pronounced temperature-dependent S-shaped peak positions and N-shaped linewidth were observed in PL spectra while increasing nitrogen concentration. The activation energy of InGaAsN/GaAs single quantum well (SQWs) is observed to decrease with nitrogen incorporation, which is contrary to the expectation of the bandgap reduction. This phenomenon suggests that the existence of defect-related nonradiative processes is due to nitrogen incorporation. The results of measurement demonstrate that the nitrogen incorporation into the InGaAsN has strong influence not only on carrier localization but also on the optical quality. In addition, the growth of high nitrogen content (5.3%) shows that the InGaAsN might be the potential candidate for long-wavelength optoelectronic devices.

PACS: 78.55.Cr; 81.15.Hi; 68.65.Fg; 68.35.Dv; 71.23.An; 78.55.Cr

Keywords: A3. MBE; A3. Single quantum well; B1. InGaAsN; B3. Long-wavelength application

1. Introduction

Long-wavelength of 1.3 and 1.55 μm optoelectronic devices such as lasers, detectors, filters and optical amplifiers are key components of present optical fiber communications because of minimum loss in this wavelength region [1]. Conventional GaAs-based materials are very attractive for optoelectronics. However, systems like InGaAs/GaAs only allow device operation out to about 1.2 μm [2]. In contrast, InP-based devices can easily operate within the desired wavelength window, but they suffer from poor thermal stability (lowering efficiency) and low refractive index contrast (hindering DBR fabrication) [3]. Therefore, many layers are required to produce high-reflectivity InP-based DBRs, presenting large growth challenges as well as introducing high series resistance, which retards device dynamics [4,5]. The quaternary alloy InGaNAs, offering several advantages over conventional narrow-gap materials, has been demonstrated to be a promising material to solve these problems [6–8]. InGaNAs quantum wells (QWs) can be grown pseudomorphically on

*Corresponding author. Tel.: +886 3 5712121x31986; fax: +886 3 5716631.
E-mail address: hckuo@faculty.nctu.edu.tw (H.C. Kuo).
[1]Fang-I Lai is now with the Department of Electronic Engineering, Ching Yun University, Chung-li 320, Taiwan.
[2]J.S. Wang is now with the Department of Physics, Chung Yuan Christian University, Chung-li 320, Taiwan.

0022-0248/$ - see front matter © 2006 Elsevier B.V. All rights reserved.
doi:10.1016/j.jcrysgro.2006.02.028

GaAs, giving strong carrier confinement (hence thermal stability), compatibility with GaAs technology (including AlGaAs/AlAs DBRs), and extensive control of bandgap energy, strain and band alignment. In most III–V materials, substituting an element for a smaller atomic radius would reduce the lattice constant and increases the bandgap. However, Weyers et al. [9] found that replacing a fraction of arsenic atoms in GaAs with smaller nitrogen atoms rapidly reduces the bandgap. In addition, nitrogen allows band alignment, lattice constant and strain to be tailored, opening up a new dimension of band engineering [10].

In fact, InGaNAs-based vertical cavity surface-emitting laser (VCSEL), Vertical-cavity semiconductor optical amplifier (VCSOA), edge-emitting laser, photodetector, light emitting diode (LED), solar cell, modulators and heterojunction bipolar transistors (HBTs) have already been demonstrated [11–24]. Commercially, extensive groups focus their researches on pushing the emission wavelength of the dilute nitride above 1.3 μm, potentially useful for long haul links [25–29]. However, it is still difficult to obtain good quality InGaAsN/GaAs QWs due to the large miscibility gap, lattice-induced strain, and low efficiency of nitrogen incorporation. Accordingly, further studies on growth of InGaAsN are required for both scientific and technological points of view.

In this work, we investigate the optical properties of InGaAsN/GaAs single quantum well (SQW) grown by molecular beam epitaxy (MBE) with various nitrogen contents from 0% to 5.3%. The effects of nitrogen contents on the temperature dependence photoluminescence (PL) spectra and carrier localization are discussed in detail.

2. Experiments

The InGaAsN samples investigated here were grown by MBE on GaAs (1 0 0) substrates in a Riber system equipped with solid-sources for group-III and arsine (As) elements, and an EPI-Unibulb radio-frequency plasma source was used for supplying active nitrogen species from ultra-high-purity N_2 gas. The plasma power and N_2 flow rate were varied from 200 to 600 W and 0.2 to 0.6 sccm, respectively. And the N composition was controlled by monitoring the intensity of the N plasma emission and calibrated from the X-ray diffraction (XRD) analysis. However, since the nitrogen incorporation efficiency is hundreds of times lower than that of As, the flow rate of nitrogen source must be higher than that of As source, making growing layers susceptible to damage. To remove the defected caused by low-temperature growth, all samples were in situ annealed at 700 °C for 10 min after GaAs cap layer was grown. Detailed MBE growth process has been described elsewhere [30].

The surface morphology of the samples was determined by in situ reflection high-energy electron diffraction (RHEED) patterns. During the growth of SQWs, the RHEED patterns remain streaky in all samples. This indicated that the three-dimensional growth mode was suppressed under suitable growth conditions even with high nitrogen composition. High resolution XRD patterns using a Bede four-crystal diffractometer were performed to characterize the structural properties. In addition, the molar fractions of indium and nitrogen were determined from the fitting results of XRD spectra using dynamic simulation software (RADS). A series of samples have been grown with varying nitrogen content while keeping the 34% indium and 66% Ga concentration. The N composition in the structures was 0%, 2.2%, 4.1% and 5.3% for samples A, B, C and D, respectively. For the PL measurements, the samples were excited by argon ion laser (532 nm), and the PL signal was collect in conventional back scattering geometry. All samples were placed into a closed-cycle cryostat with a temperature controller ranging from 20 K to room temperature. And the luminescence signal was dispersed by a Spex Triax 320 monochromator and detected by a thermoelectrically cooled InGaAs detector.

3. Results and discussion

Shan et al. [31] have proposed a band anticrossing (BAC) model to describe the nitrogen and indium concentration dependence of the effects on the bandgap of the InGaAsN alloy system. According to the model, the band gap of InGaAsN can be expressed as

$$E_g(\mathrm{In}_x\mathrm{Ga}_{1-x}\mathrm{As}_{1-y}\mathrm{N}_y) = \frac{E_M(x)+E_N-\sqrt{[E_M(x)-E_N]^2+4V_{NM}^2(x,y)}}{2}, \quad (1)$$

where the top of the valence band is taken as a reference energy level, E_M is the extended conduction band of the InGaAs ternary compound, E_N is an impurity level due to nitrogen incorporation assumed here to be located 1.65 eV above the valence band, and V_{NM} represents the degree of interaction between the E_N and E_M levels [32]. The theoretical model based on a BAC model interaction between the highly localized nitrogen-derived state and the zone-center conduction band Bloch states has been constructed and used to explain the band-gap behavior, including pressure and temperature dependence, for bulk dilute nitrides including GaNAs, GaInNAs, and GaNP. However, the extent to which this model accurately describes the underlying physics of this new class of material is still unclear. The band gap energies of samples A, B, C, and D, calculated using Eq. (1), are for references. Due to the quantum confinement effect, the measured band gap energies are larger than the calculated results.

Fig. 1 shows temperature-dependent PL spectra of the four samples. PL emission from high quality quantum well and bulk samples is typically characterized by symmetric, Gaussian-like, features as illustrated for InGaAs and GaAs. However, emission from dilute nitride samples is often characterized by asymmetric peaks with low-energy

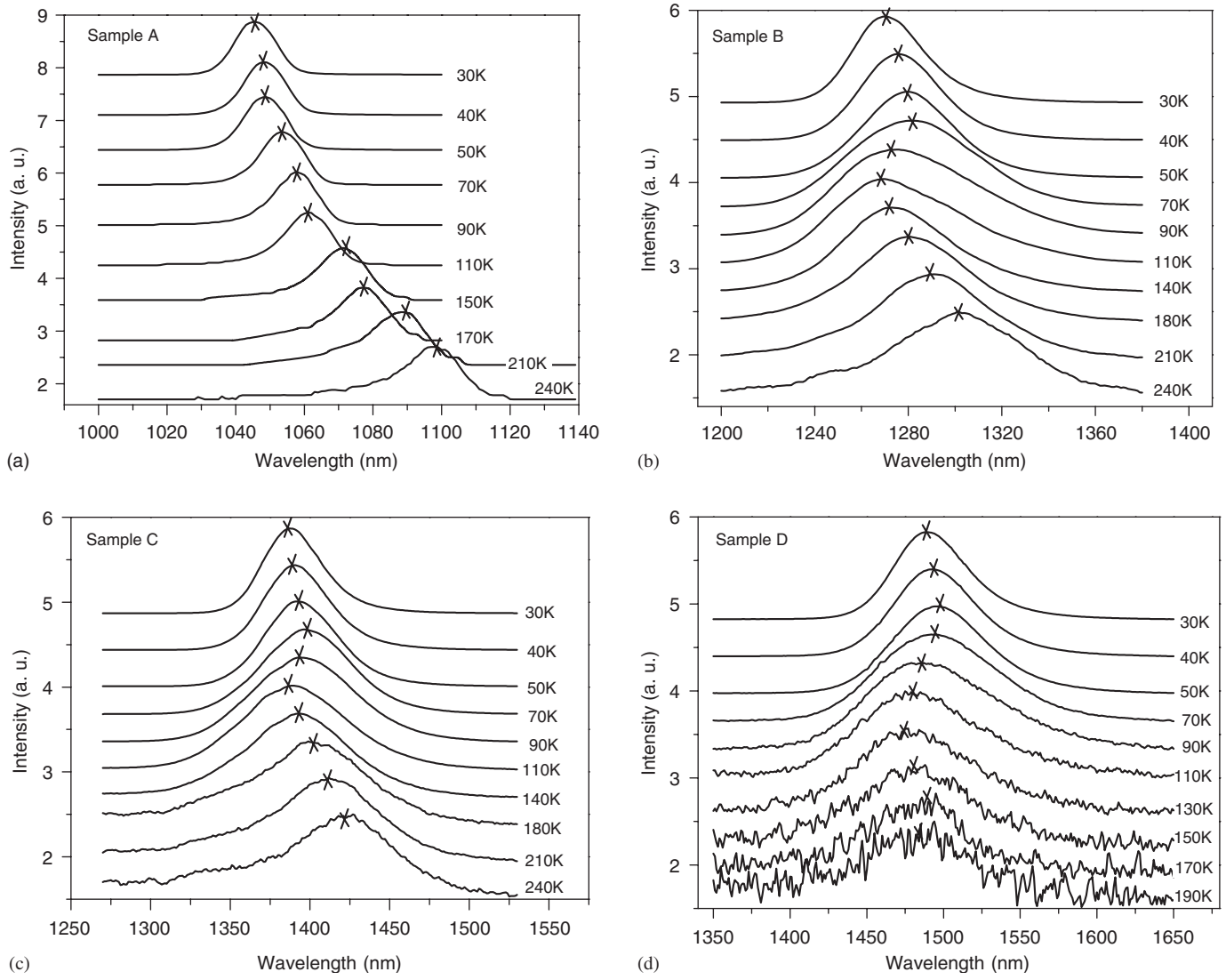

Fig. 1. The temperature dependent of the PL spectra of (a) sample A (N = 0%), (b) sample B (N = 2.2%), (c) sample C (N = 4.1%) and (d) sample D (N = 5.3%). The signs are marked on the peak of the spectra.

exponential tails [33–35]. The PL spectra in Fig. 1 exhibit conspicuous asymmetric line shapes with sharp high-energy cutoff and exponential low-energy tail with nitrogen incorporation. The form of the low energy side of the spectrum suggests a distribution of localized states with an exponential-like density of states (DOS). These tail states might originate from recombination of localized excitons trapped in potential fluctuations due to local fluctuations in nitrogen concentration. In addition, with increasing nitrogen concentrations (from sample A to sample D), the emission peak positions show a remarkable red-shift tendency as predicted from Eq. (1) at low temperature (~20 K). As shown in Fig. 1(a) for sample A, only one symmetrical emission peak centered on around 1046 nm was observed and the peak energy redshifts while increasing the temperatures. This phenomenon is in agreement with a regular thermalization of the carriers, where the localization energy is equal to zero. Particularly, other samples exhibit an anomalous temperature behavior. The behavior differs remarkably from the change of the band gap energy with temperature usually described by the Varshni formula (as shown in Fig. 2(a)) [36]. The so-called S-shaped temperature dependence of emission energy, i.e. a red-blue-red shift with increasing temperature, was observed in the samples B and C with higher nitrogen content. Band tail states were proposed should be responsible for the InGaAsN system [37–39]. Other than the reference sample A without nitrogen, the anomalous temperature-induced emission shifts in sample B and C are attributed to band tail states in DOS. From Fig. 1, changing nitrogen content from 0 to 0.05 reduces the band-gap energy. Also, a correlation between PL linewidth and nitrogen concentration was exhibited, which the PL linewidth is broadening with the increase of N incorporation. This broadening phenomenon indicates that an increasing degree of compositional and structural disorder with

increasing nitrogen concentration deteriorate the crystal quality in the quantum wells, which has been extensively reported.

The temperature dependence of the peak energy is depicted in Fig. 2 for the four samples (sample A–D). The solid lines represent the fitting results in the high-temperature range using empirical Varshni model [36]

$$E(T) = E(0) - \frac{\alpha T^2}{T + \beta}, \tag{2}$$

where the $E(0)$, α and β are Varshni parameters, and T is the measured temperature. All fitting parameters are given in Table 1. According to Table 1, we found that the thermal stability of PL peak energy increases (value of α decreases and β increases) with increasing N content, which is consistent with earlier reports. The carrier localization energy at any temperature is given by the difference $E_{loc}(T) = E(T) - E_{PL}(T)$, where $E_{PL}(T)$ is temperature dependence of PL peak energy [39]. The results of the Varshni fit and the localization energies at 20 K for all samples are shown in Fig. 2 as well. In Fig. 2(a), a superposition of the Varshni fit and experimental data indicates that the evolution of the PL peak position for the InGaAs (reference sample A) is in agreement with a regular thermalization of the carriers, where the localization energy is equal to zero [40]. It is interesting to note that the temperature dependent PL of sample B, C and D exhibit an S-shaped property. At the lowest temperature, the photo-generated carriers (excitons), captured by the localized potential induced by the fluctuation of well width or alloy composition, are essentially immobile apart from phonon-assisted tunneling or hopping to adjacent states. With the increase of the temperature from 20 K to first minimum, a redshift appears because of the excitons gain sufficient thermal energy to overcome small potential barriers and thus are mobile to some extent. In this case, some of these excitons may relax down into and become trapped in the lower energy levels where the recombination takes place. Consequently, the emission of the high energy states is suppressed and a redshift occurs within the range. However, with the further increase in temperature, a blue shift of peak energy occurs. This blue shift could be owing to the thermal equilibrium distribution of the localized excitons increasing and getting close to the delocalized higher energy states of DOS [8]. At even higher temperature, the temperature-dependence peak energy is mainly dominated by the behavior of the band-to-band transition and the peak energy will decrease as the thermal shrinkage of gap energy. Besides, it is obviously that the linewidth increases accordingly when increasing the temperature above 20 K. Additionally, earlier literatures have pointed out that the incorporation of nitrogen into the InGaAs increases the density of defects originated from compositional and structural inhomogeneities, and deteriorates the crystalline quality. So it is reasonable that sample D did not manifest pronounced S-shape feature due to lower signal-to-noise ratio (SNR) and measurable temperature. The localization energies at 20 K for all samples are summarized in Table 1. From the figure, we observed that N content has an influence on carrier localization in the investigated QW systems.

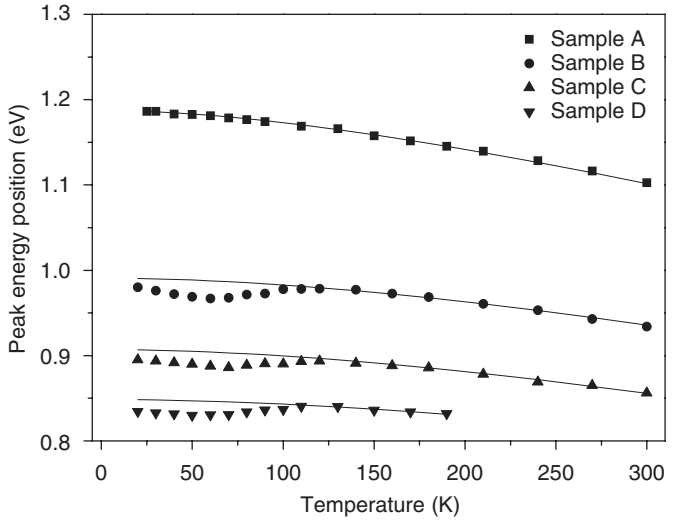

Fig. 2. Evolution with the temperature of the PL-peak energies for the (a) sample A (N = 0%), (b) sample B (N = 2.2%), (c) sample C (N = 4.1%) and (d) sample D (N = 5.3%). The solid lines are the fitting results in the high-temperature range using empirical Varshni model.

Fig. 3 shows the temperature dependence of the PL linewidth. For sample A without nitrogen content, the value of FWHM increases monotonically from 13 to 26 meV. The spectral linewidth increases with temperature should be result from thermal broadening in the absence of tail states, and therefore the band-to-band transition luminescence FWHM usually depends linearly on temperature [41]. Hence, the recombination in sample A is supposed to be band-to-band like. On the other hand, the PL linewidth of samples B and C increase till temperature close to the delocalization temperature (~100 K). However,

Table 1
Characteristics of the samples: the molar fraction of nitrogen were determined from the fitting results of XRD spectra, E_{loc} (20 K) represents the localization energy at 20 K, E_0, α, and β are the Varshni parameters

Sample	Nitrogen composition (%)	E_{loc} (20 K) (meV)	E_0 (eV)	α (10^{-4} meV/K)	β (K)
A	0	~0	1.1872	5.8	310
B	2.2	10.3	0.9907	5.35	575
C	4.4	11.6	0.907	5.1	585
D	5.3	13.7	0.8485	4	650

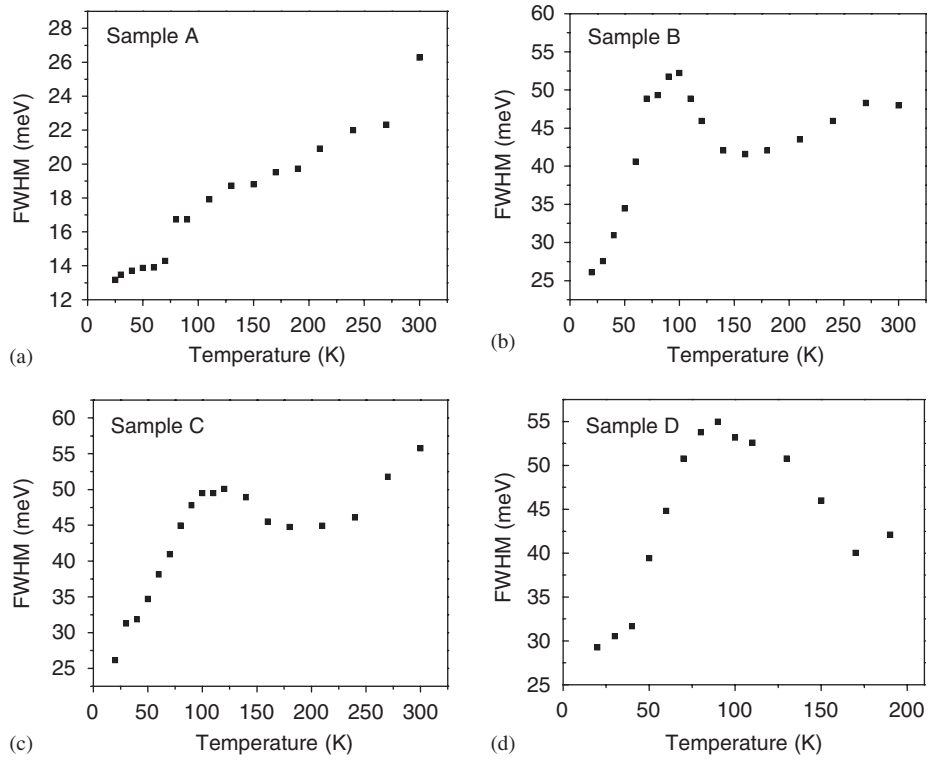

Fig. 3. Temperature dependence of the PL linewidth for the (a) sample A (N = 0%), (b) sample B (N = 2.2%), (c) sample C (N = 4.1%) and (d) sample D (N = 5.3%).

as the temperature increase from 100 to 150 K, the value of FWHM decreases from 50 to 40 meV. Finally, the linewidth rises up steadily to 300 K, again in agreement with a regular thermalization of the carriers. This N-shaped temperature evolution could be explained by the transfer and thermalization of localized states [39]. When the temperature increases up to the thermalization point, some localized carriers become mobile and occupy shallower localized states. This leads to an increase of the linewidth. When approaching the full-delocalization temperature, most localized carriers become progressively mobile and occupy shallower localized states, so that the carrier distribution stabilizes and narrows the emission linewidth. Further, thermal broadening of the carrier distribution occurs and the linewidth increases with increasing the temperature accordingly. As mentioned above for sample D with high nitrogen content (5.3%), the deteriorated optical property results in ambiguous N-shaped temperature dependence.

Finally, the temperature dependence of normalized integrated intensity of PL was investigated. The curves of normalized integrated PL intensity versus the inverse temperature for all samples were plotted in Fig. 4. With an increase in temperature, the overall integrated emission intensity of the PL spectra gradually decreases indicating the presence of nonradiative recombination centers. The quenching behavior should correspond to the thermal activated nonradiative recombination mechanism, where the slopes give the activation energy. For proper fitting,

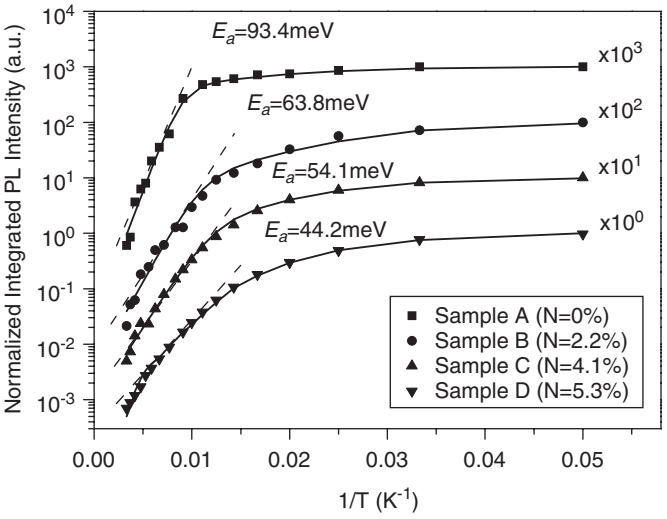

Fig. 4. Curves of normalized integrated PL intensity versus the inverse temperature for (a) sample A (N = 0%), (b) sample B (N = 2.2%), (c) sample C (N = 4.1%) and (d) sample D (N = 5.3%). The solid lines are the activation energy E_a.

two thermally activated energies characterized by E_a and E_b were assumed using the following formula [42]

$$I(T) = \frac{1}{1 + A\exp\left(\frac{-E_a}{kT}\right) + B\exp\left(\frac{-E_b}{kT}\right)}, \quad (3)$$

where A and B are fitting constants; and k is the Boltzmann constant. It is found that the values of E_b for all samples, determined by curve fitting, are in the range of 8–13 meV. Also, the E_b values increase with increasing N concentration and closely correlate with measured E_{loc} values. Hence, the small activation energy of E_b is attributed to trapped excitons or carriers thermalizing from localized regions resulting from potential fluctuation in the SQWs. Besides, the activation energy E_a, derived from the slopes of the straight-line portion (150–300 K) of the curves, is 93.4, 63.8, 54.1 and 44.2 meV for nitrogen compositions of 0%, 2.2%, 4.1% and 5.3%, respectively. The E_a values decrease with increase of nitrogen incorporation. This fitting result is contrary to the expectation of E_a value which would increase as increasing nitrogen content due to bandgap reduction. These features might attribute to different samples and excitation conditions since the recombination dynamics should be dependent on the distribution of localized states. Furthermore, the decrease of E_a can be explained by a higher defect concentration owing to more nitrogen incorporation thus leading to a stronger influence of the defect-related nonradiative processes.

4. Conclusion

In conclusion, the optical properties of $In_{0.34}Ga_{0.66}As_{1-x}N_x$/GaAs SQWs grown by solid-source MBE with various nitrogen contents were investigated by temperature-dependent PL. The PL peak energy and FWHM exhibit pronounced temperature-dependent S-shape N-shape while increasing nitrogen concentration. Moreover, the band-tail states, which might originate from composition nonuniformity, play a key role on the carrier localization effect in the nitrogen-incorporated samples, and the nitrogen contents should be responsible for the localization energy. The activation energy E_a of InGaAsN SQW is observed to decrease with nitrogen incorporation, contrary to the expectation of the bandgap reduction. This feature suggests that the existence of defect-related nonradiative processes due to nitrogen incorporation. All aforementioned results indicate that the nitrogen contents have strong influence on the optical properties of the InGaAsN/GaAs SQW. Furthermore, the highest nitrogen concentration obtained here is 5.3%, and the emission wavelength reaches 1.5 μm as well. Although the optical qualities deteriorate while increasing nitrogen contents, our results indicate that InGaAsN/GaAs SQW is potential candidate for long-wavelength optoelectronic devices.

Acknowledgment

The authors would like to thank M. Y. Tsai J. P. Chu and Y. H. Chang in National Chiao-Tung University, Taiwan and N. Tansu in Lehigh University, USA for useful discussion. The authors would also like to thank A. R. Kovsh in A. F. Ioffe Institute Russia and Opto-Electronics & Systems Laboratories of the Industrial Technology Research Institute (ITRI), Taiwan for technical discussion. This work was supported in part by National Science Council of Republic of China (ROC) in Taiwan under contract No. NSC 93-2215-E-009-063 and by the Extend Academic Excellence Program of the ROC under the contract No. NSC. 93-2752-E-009-008-PAE, and by the MediaTek Fellowship.

References

[1] M. Kondow, K. Uomi, A. Niwa, T. Kitatani, S. Watahiki, Y. Yazawa, Japan J. Appl. Phys. 35 (1996) 1273.
[2] S. Sato, S. Satoh, Japan J. Appl. Phys. 38 (1999) L990.
[3] M. Kondow, T. Kitatani, S. Nakatsuka, M. Larson, K. Nakahara, Y. Yazawa, M. Okai, IEEE J. Sel. Top. Quant. Electron. 3 (1997) 19.
[4] J.J. Dudley, D.I. Babic, R. Mirin, L. Yang, B.I. Miller, R.J. Ram, T. Reynolds, E.L. Hu, J.E. Bowers, Appl. Phys. Lett. 64 (1994) 1463.
[5] B.I. Babic, K. Streubel, R.P. Mirin, M.N. Margalit, E.L. Hu, J.E. Bowers, D.E. Mars, L. Yang, K. Carey, IEEE Photon. Technol. Lett. 7 (1995) 1225.
[6] M. Kondow, S. Nakatsuka, T. Yazawa, M. Okai, Japan J. Appl. Phys. 35 (1996) 5711.
[7] M. Reinhardt, M. Fisher, A. Forchel, Physica E 7 (2000) 919.
[8] H.D. Sun, M. Hetterich, M.D. Dawson, A.Yu. Egorov, D. Bernklau, H. Riechert, Appl. Phys. Lett. 92 (2002) 1380.
[9] M. Weyers, M. Sato, H. Ando, Japan J. Appl. Phys. 31 (1992) L853.
[10] G. Leibiger, V. Gottschalch, M. Schubert, J. Appl. Phys. 90 (2001) 5951.
[11] A.R. Kovsh, J.S. Wang, R.S. Hsiao, L.P. Chen, D.A. Livshits, G. Lin, V.M. Ustinov, J.Y. Chi, Electron. Lett. 39 (2003) 1726.
[12] H.C. Schneider, A.J. Fischer, W.W. Chow, J.F. Klem, Appl. Phys. Lett. 78 (2001) 3391.
[13] M. Kawaguchi, T. Miyamoto, E. Gouardes, D. Schlenker, T. Kondo, F. Koyama, K. Iga, Japan J. Appl. Phys. 40 (2001) L744.
[14] A. Ramakrishnan, G. Steinle, D. Supper, C. Degen, G. Ebbinghaus, Electron. Lett. 38 (2002) 322.
[15] J.B. Heroux, X. Yang, W.I. Wang, Appl. Phys. Lett. 75 (1999) 2716.
[16] G.S. Kinsey, D.W. Gotthold, A.L. Holmes Jr., J.C. Campbell, Appl. Phys. Lett. 77 (2000) 1543.
[17] T. Kato, Y. Mizuno, M. Hirotani, T. Saka, H. Horinaka, J. Appl. Phys. 89 (2001) 2907.
[18] S.R. Kurtz, A.A. Allerman, E.D. Jones, J.M. Gee, J.J. Banas, B.E. Hammons, Appl. Phys. Lett. 74 (1999) 729.
[19] J.F. Geisz, D.J. Friedman, Semicond. Sci. Technol. 17 (2002) 769.
[20] A. Balcioglu, R.K. Ahrenkiel, D.J. Friedman, Appl. Phys. Lett. 76 (2000) 2397.
[21] Y.S. Jalili, P.N. Stavrinou, J.S. Roberts, G. Parry, Electron. Lett. 38 (2002) 343.
[22] P.C. Chang, A.G. Baca, N.Y. Li, P.R. Sharps, H.Q. Hou, J.R. Laroche, F. Ren, Appl. Phys. Lett. 76 (2000) 2788.
[23] P.C. Chang, A.G. Baca, N.Y. Li, M. Xie, H.Q. Hou, E. Armour, Appl. Phys. Lett. 76 (2000) 2262.
[24] N.Y. Li, P.C. Chang, A.G. Baca, X.M. Xie, P.R. Sharp, H.Q. Hou, Electron. Lett. 36 (2000) 81.
[25] M. Fischer, M. Reinhardt, A. Forchel, Electron. Lett. 36 (2000) 1208.
[26] M. Fischer, D. Gollub, M. Reinhardt, M. Kamp, A. Forchel, J. Crystal Growth 251 (2003) 353.
[27] K.C. Yew, S.F. Yoon, Z.Z. Sun, S.Z. Wang, J. Crystal Growth 247 (2003) 279.
[28] S. Makino, T. Miyamoto, M. Ohta, T. Matsuura, Y. Matsui, F. Koyama, Conference Proceedings—International Conference on Indium Phosphide and Related Materials, 2003, pp. 460–463.
[29] M. Fischer, M. Reinhardt, A. Forchel, IEEE J. Sel. Top. Quant. Electron. 7 (2001) 149.

[30] J.S. Wang, A.R. Kovsh, R.S. Hsiao, L.P. Chen, J.F. Chen, T.S. Lay, J.Y. Chi, J. Crystal Growth 262 (2004) 84.
[31] W. Shan, W. Walukiewicz, J.W. Ager III, E.E. Haler, J.F. Geisz, D.J. Friedman, J.M. Olson, S.R. Kurtz, Phys. Rev. Lett. 82 (1999) 1221.
[32] A. Lindsay, E.P. O'Reilly, Solid State Commun. 112 (1999) 443.
[33] I.A. Buyanova, W.M. Chen, G. Pozina, J.P. Bergman, B. Monemar, H.P. Xin, C.W. Tu, Appl. Phys. Lett. 75 (1999) 501.
[34] Z. Pan, L.H. Li, W. Zhang, Y.W. Lin, R.H. Wu, W. Ge, Appl. Phys. Lett. 77 (2000) 1280.
[35] R.A. Mair, J.Y. Lin, H.X. Jiang, E.D. Jones, A.A. Allerman, S.R. Kurtz, Appl. Phys. Lett. 76 (2000) 188.
[36] Y.P. Varshni, Physica (Utrecht) 34 (1967) 149.
[37] A. Kaschner, T. Lüttgert, H. Born, A. Hoffman, A.Y. Egorov, H. Riechert, Appl. Phys. Lett. 78 (2001) 1391.
[38] L. Grenouillet, C. Bru-Chevallier, G. Guillot, P. Gilet, P. Duvaut, C. Vannuffel, A. Million, A. Chenevas-Paule, Appl. Phys. Lett. 76 (2000) 2241.
[39] M.A. Pinault, E. Tournie, Appl. Phys. Lett. 78 (2001) 1562.
[40] J. Misiewicz, P. Sitarek, K. Ryczko, R. Kudrawiec, M. Fischer, M. Reinhardt, A. Forchel, Microelectron. J. 34 (2003) 737.
[41] S. Iyer, S. Hegde, A.A. Fadl, K.K. Bajaj, W. Mitchel, Phys. Rev. B 47 (1993) 1329.
[42] J.D. Lambkin, L. Considine, S. Walsh, G.M. O'connor, C.J. McDonagh, T.J. Glynn, Appl. Phys. Lett. 65 (1994) 73.